Developing continuous submicron-scale conductive interpenetrating hydrogel network in polyethylene matrices through controlled crazing and polymerization

Anton Kornberg,[a] *Michael Thompson,*[b] *Shiping Zhu* [ab]*

[a] Department of Chemical Engineering, McMaster University, Hamilton, Ontario, Canada

[b] School of Science and Engineering, The Chinese University of Hong Kong, Shenzhen, Guangdong, China 518172.

* Author to whom correspondence should be sent. E-mail: shipingzhu@mcmaster.ca

Keywords: conductivity, polyethylene, acrylate, co-continuous structure, crazing, tensile deformation, surface-active medium.

ABSTRACT

An approach is described for the synthesis of controlled submicron interpenetrating networks with distinct functional features in commodity polymers, based on a mechanism of crazing and polymerization. In this work, ion conductivity was introduced into polyethylene with only minor

losses in its mechanical properties, using a highly branched acrylic hydrogel. Control over the porous network developed in the matrix was gained by the addition of a crystallizing nucleating agent, which was used to increase the number and reduce the size of crystallites. Variation of experimental conditions, such as the degree of elongation and applied reaction pressure, produced different morphologies and conductivity for the co-continuous alloy. The samples were deformed in a liquid medium that possessed an affinity for the matrix material, and acted both as a surface-active agent for the crazing, and as a reactant for the conductive phase. Without pressure, deforming by 100% strain yielded a conductivity of 5.67×10^{-7} S/cm for the polymer specimen. Simultaneously increasing system pressure while constantly straining a specimen enabled further enhancements in conductivity. As a particular example, elongation of 100% and applied pressure up to 2.76 MPa ensured conductivity nearly equal to that of the pure hydrogel at 4.43×10^{-4} S/cm.

1. INTRODUCTION

In recent years, hydrogels have attracted significant interest for bioengineering applications, due to their capacity to mimic biological communication. The majority of biological signaling is mediated by ions, and hydrogels function in the same way by transmitting ions via counter-ions embedded in the polymer network. Control over such processes is carried out by adjustable electrical stimuli that release molecules on-demand, with defined intensity and frequency.[1–3] However, applications of hydrogels are often limited due to their weak mechanical properties while swollen, which is necessary for their function.[4] In nature, gentle tissues are normally supported by an extracellular fibrous protein framework, and their mechanical properties therefore are less critical. Other supporting network structures applicable to synthetic hydrogels

have included nanofibers,[5–7] surgical sutures,[8] or highly-porous electrospun matrices,[9,10] all expensive systems to manufacture. The present research investigates a generalized approach for introducing value-added functionality with nano-to-micron scaled features in a broad range of matrix polymers, by polymerizing a secondary polymer phase within newly creating pores produced along crystallite boundaries during plastic deformation. The introduced hydrogel in this case was polymerized within the continuous submicron network that percolated through the matrix, to demonstrate through-plane conductivity, while the matrix itself acted as a mechanically durable scaffold.

The fracture mechanism that is induced in the demonstrated method is similar to the one that occurs naturally during Environmental Stress Cracking (ESC), for which a polymer experiences crack propagation under stress while drawing in a surround liquid deeper into the material. This type of chemical influenced deformation was studied earlier by Bernier and Kambour,[11] and later adopted for practical uses by Volynskii et al.,[12,13] and Rozanski et al.[14] Both of the latter research groups showed that samples subjected to tensile deformation in a liquid media, formed a large number of submicron crazes that percolated through the polymer film. Subsequent studies by Rozanski et al. reported on the significance of crystallinity on the network of crazes by this procedure.[15] The authors investigated the resulting samples by X-ray and thermal analyses, showing that the crystal fraction was unaffected by the deformation.

Attempts to use this mechanism to create two-component systems have been reported earlier. In the study by Weichold et al.[16] and Trofimchuk et al.,[17] the authors used a liquid medium, in which the samples were deformed, as a carrier for nonvolatile additives that remained inside the bulk polymer after the medium evaporated. Rukhlya et al.[18,19] used a similar method to fabricate a two-component alloy by deformation high-density polyethylene (HDPE) matrices within a

solution of polyethylene oxide (PEO) in ethanol. The authors varied the deformation regimes, such as percentage of elongation and deformation rate, and then examined how it affected the volume of absorbed PEO. Those studies did not characterize the morphology of the ally nor characterized the extent to which an interpenetrating structure was formed. Yarysheva et al.[20] applied the same technique, adopted from the research of Rukhlya. Using X-ray spectral analysis, the authors showed a uniform distribution of oxygen atoms throughout the bulk volume attributed to the PEO though still there was no consideration whether the filled pores were interconnected or much less, formed a percolating network which would add far more functionality to a material. For all of these reported systems, the viscosity of the fluid was increased by the dissolved or suspended secondary phase which diminished its likelihood of fully penetrating all of the pores created by crazing. It is our belief that *in situ* polymerization of the secondary phase addresses this problem and would allow co-continuous properties to be developed with little loss in the mechanical properties of the matrix.

Therefore, the present research aimed to devise a modified approach based on polymerization to attain a sub-micron interpenetrating structure to introduce new functionality in the final alloy while minimizing mechanical losses. An important criterion for the approach was the monomeric liquid medium, in this case used to introduce ion conductivity, had to also possess a surface-active functionality with the polyethylene matrix to influence crazing so the process consisted of one step for simplicity. The study examined the extent of longitudinal elongation and reaction system pressure to achieve the chief objectives of a percolating network for the secondary phase.

2. EXPERIMENTAL METHODS

2.1. MATERIALS

Linear low-density polyethylene (LLDPE LL 8460.29 powder, ExxonMobil Chemical) and titanium dioxide nanoparticles (TiO_2 P25 AEROXIDE, Degussa) were used as received. The TiO_2 had an average particle size of 21 nm. Acrylic acid (AAc, 99%, Aldrich) was purified of its inhibitor before use. 2,2′-Azobis (2-methylpropionitrile) (AIBN, 98%, Aldrich) was recrystallized from methanol before use. N,N′-Methylenebis (acrylamide) (MBA, 99%, Aldrich) and ethanol anhydrous (EA, ≤0.005% water) were used as received.

2.2. PREPARATION OF P(AAc-co-MBA)

In this study, a cross-linked poly(acrylic acid) was chosen as the model ion-conductive polymer due to its ease of synthesis and high affinity of the acrylic acid monomeric precursor to the matrix polymer (LLDPE). Along with AAc monomer, the recipe included 3 wt% MBA as the cross-linking agent and 1 wt% AIBN as the initiator. The resulting mixture was sonicated and cooled down to 0 °C to avoid spontaneous polymerization. Before use as a liquid medium, the recipe was premixed with 30 vol% of EA. This ratio ensured the smallest possible contact angle of 16.1 ± 0.4° to the matrix polymer surface at the highest concentration of AAc.

2.3. PREPARATION OF MATRIX SAMPLES

Before use, the LLDPE powder (35 mesh) was premixed with 2 wt% of TiO_2 nanoparticles. Dumbbell-shaped polyethylene samples of 110±10 μm thickness, with the narrow section being 5 mm long and 5 mm wide, were molded in a hot press at 200 °C and 6 bars for 5 minutes and then cooled.

2.4. DEFORMATION OF SAMPLES AND POLYMERIZATION IN HIGH-PRESSURE REACTOR

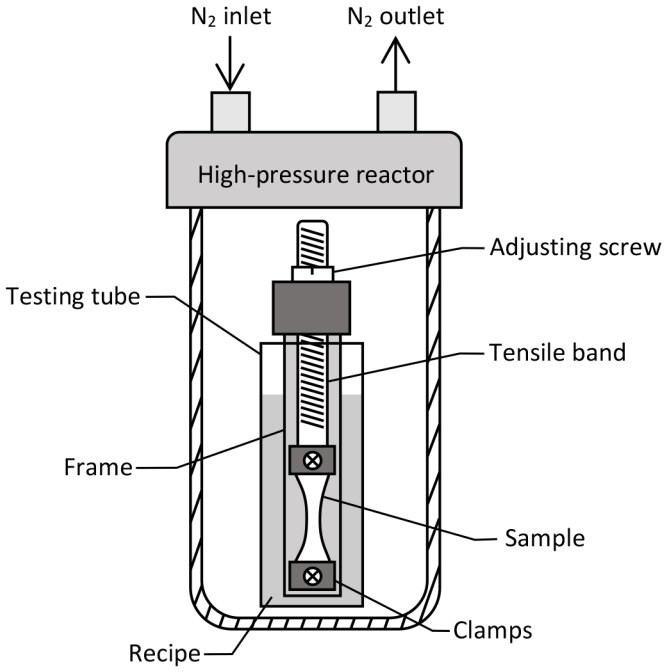

Figure 1. Schematic design of the tensile rig while the sample is mounted and immersed in the medium.

A tensile rig was designed to apply uniaxial strain to the samples while immersed in the monomeric medium (Fig. 1). The rig was contained inside a high-pressure reactor, which was frequently depressurized to step-wise deform a sample followed by purging with nitrogen and subsequently pressurizing to an experimentally varied setpoint. For the samples deformed at atmospheric pressure, the reactor was only purged with nitrogen, without pressurization. Step changes in the extent of deformation were done at 0.25 mm per cycle increments, so that the resulting elongation rate was kept constant at 0.03 $mm \cdot min^{-1}$. The deformation was carried out

until the degree of longitudinal elongation reached 25, 50, 75 or 100% strain. Deformation was performed at ambient room temperature. Each set of experimental conditions was applied for a minimum of three repeats.

For polymerization, the reactor containing the tensile rig was moved into an oven set to 80 °C and heated for 3 hrs under the given pressure. Measurements inside the reactor showed that the temperature was equalized with the temperature of the oven after 15 minutes when its internal pressure was zero, and in less time when the pressure was increased. The sample remained under strain and immersed in the same medium. After polymerization, the samples were released from the tensile rig and scrapped clean of any hydrogel at the surface of the sample. Then, the samples were held under vacuum at 40 °C for 24 hours, to remove any monomer residues.

The experimental parameters for these trials are listed in Table 1. Samples were named according to the applied pressure (capital letters from A to E, where A is the highest pressure of 2.76 MPa, and F is atmospheric pressure) and the percent strain. For example, the sample denoted as A75 was deformed at 2.76 MPa to 75% strain. Elongation length of a sample was determined at the middle-narrowed part of the dumbbell-shaped sample, since this section experienced the highest stresses. For example, when a sample had elongated by 75% this narrowed region increased in length by 3.75 mm, while the sample increased by 8.75 mm in total. Samples deformed while immersed in the monomer without any initiator were denoted as "NI".

Table 1. Conventional symbols of the samples according to the experimental conditions.

Elongation, % / **Pressure, MPa (psi)**	**25**	**50**	**75**	**100**
2.76 (400)	A25	A50	A75	A100
2.41 (350)	B25	B50	B75	B100
2.07 (300)	C25	C50	C75	C100
1.72 (250)	D25	D50	D75	D100
1.38 (200)	E25	E50	E75	E100
atmospheric	F25	F50	F75	F100
"no initiator" 2.76 (400)	NI25	NI50	NI75	NI100

2.5. ION CONDUCTIVITY MEASUREMENT

After vacuum drying, samples were immersed in a 1M aqueous NaOH solution for 48 hrs, in order to neutralize the carboxylic acid groups. The samples were then washed with deionized water, dried, and weighed. Each dried sample was polished by sandpaper and cropped into a rectangular shape, to avoid ion transport circumventing the intended path through the sample. The resulting rectangular specimen was immersed for 12 hrs in the aqueous NaOH solution again for electrolyte saturation, wiped dry and then sealed in place by molten wax over top of a cut out opening in a polystyrene dish. The dish was filled with aqueous NaOH and was immersed in a dish of a larger diameter, also filled with aqueous NaOH. The design of the measurement cell prevented leaks and guaranteed ion transport only through the embedded specimen.

Resistivity ϱ was calculated by the formula $\varrho = (R \cdot A)/L$, where R was the measured resistance by an Agilent 34401A 6½ Digit Multimeter. Two electrodes, both of the same area A, were made from copper foil and affixed to both exposed sides of the specimen but not sealed in place so as to hinder electrolyte wetting of the specimen. Technically, the distance between the electrodes was slightly greater than the thickness of the specimen. However, since R of the electrolyte was much less than that of the specimen, the specimen thickness was taken as dimension L. The DC bulk conductivity σ [$S \cdot cm^{-1}$] was calculated as $\sigma = 1/\varrho$.

Continuous agitation of the cell, as well as the careful maintenance of pH at 13.7 by adding fresh electrolyte, minimized signal drift during the measurement. To maintain the consistency of the results, the R values were always taken ten seconds after the closure of the measurement loop.

2.6. MECHANICAL CHARACTERIZATION

Strain-controlled tensile testing was performed using a benchtop Model 3366 Universal Mechanical Testing System with a 5 kN load cell (Instron Corporation; Canton, MA), at ambient room temperature. Before testing, the thickness was measured with a caliper at three points in the narrow sample section. The samples were pulled longitudinally at a crosshead speed of 2.5 $mm \cdot min^{-1}$ until failure.

2.7. SURFACE MORPHOLOGY ANALYSIS

Samples were cryogenically fractured in the middle of the narrow section. Micrograph images were obtained by JEOL JSM 7000 scanning electron microscope (SEM). Platinum was used to deposit a conductive layer of 5 nm thickness. After microscopy, the SEM images were processed

using ImageJ software (National Institute of Health, U.S.) to determine individual void sizes by detecting their contours based on about five hundred iterations for each image.

2.8. ATR-FTIR CHARACTERIZATION

Mid-range infrared spectra from 1000–3500 cm^{-1} were recorded using a Thermo Nicolet 6700 bench with DTGS detector and diamond-window attenuated total reflectance (ATR) attachment, by scanning 64 times at a resolution of 2 cm^{-1}. The samples were progressively sectioned using a manual rotary microtome (Leica Biosystems) to an ultimate depth of 50 μm (approximately half of the total sample thickness), along the longitudinal axis. Right before scanning, the samples were immersed in deionized water for several seconds. Visible excess water was removed by using the glass surface. Water was absorbed in the acrylate phase, swollen within the void space so that the acrylate polymer was more readily detected in the scans.

3. RESULTS AND DISCUSSION

3.1. RESULTING MORPHOLOGY

According to several fracture studies,[21,22] primary voids emerge in large quantities at the crystal-amorphous interface due to chain depletion in the amorphous phase during crystallization. Bucknall[23] and later, Pawlak et al.[24] established that cavitation initiated at these primary voids during deformation will ultimately propagate as crazes. These crazes present themselves as a porous network in the deformed material. By extension of these studies,[21–24] increasing the crystal-amorphous interfacial area should increase the number of primary voids, creating circumstances where an equivalent cross-sectional cavity area is produced by smaller sized crazes. Hypothetically, sufficiently small crazes should create a space for the conductive secondary phase in our new material with minimal influence on the stiffness of the matrix.

In order to increase the crystal-amorphous interface, the number of crystallites per unit area was increased by adding 2 wt% of TiO_2 nanoparticles as a crystal nucleating agent during the sample preparation for all trials. Polarized light optical micrographs in Fig. 2 show the difference in the crystal structures of pure polyethylene versus polyethylene with added nanoparticles. As a result of the nucleating agent, instead of the large spherulites found in the original material (greater than 10 μm in size), the modified polyethylene matrix contained a larger number of smaller crystallites with sizes of 1 μm or less.

The influence of the crystal structure was noticeable on sample deformation. In preliminary testing it was observed that only samples with the higher crystal-amorphous interfacial area (Fig. 2b) could possibly be stretched uniformly without necking, even for strains beyond the yield point of the matrix. Depending on whether the sample was stretched in air or in a medium with surface activity towards the matrix, necking occurred well beyond the yield point or not at all. According to Volynskii et al.,[13] such behavior indicates microfibrillation due to the formation of numerous crazes in the matrix. For the pure polyethylene samples, necking occurred at the yield point with noticeable whitening.

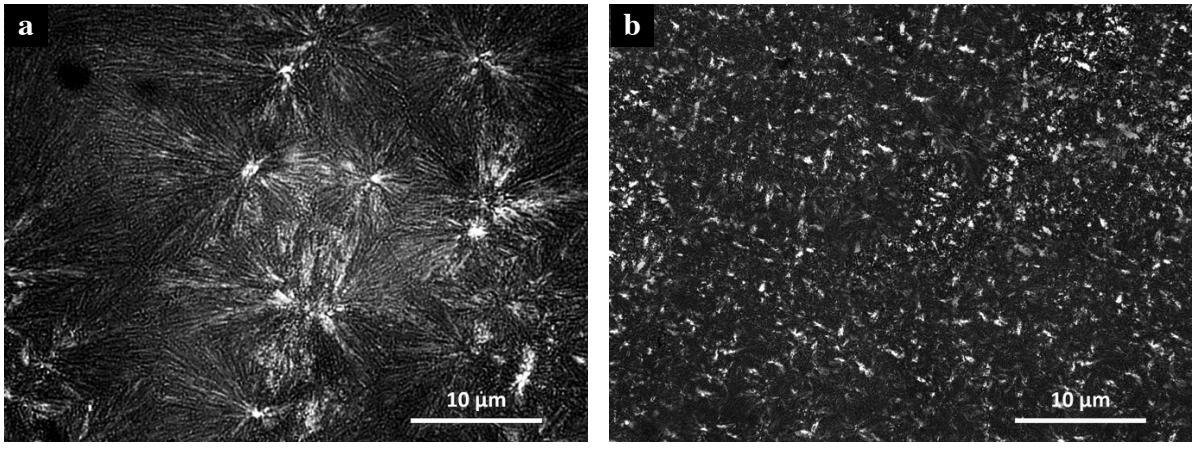

Figure 2. Crystal structure of (a) pure polyethylene, and (b) with the addition of 2 wt% TiO_2 nanoparticles, obtained by polarized light microscopy.

The extent of cavitation in the matrices was examined by SEM in Fig. 3, comparing the morphology of F100 (no pressure) and A100 (maximum pressure). The micrograph for F100 show a well-established arrangement of pores in the fractured plane being retained after deformation and polymerization of the secondary phase. Based on image analysis, the total void area was 35% for F100, with a pore size being in the order of 0.1-1.0 μm in diameter. It is expected that this structure contained some amount of dispersed hydrogel in the pore, though not seen, which supported the cellular morphology and prevented its reversed deformation after removal from the reaction tensile rig. By contrast, the samples of trials NI (not shown) displayed noticeable shrinkage once removed from the vessel, since the monomer liquid being devoid of initiator, evaporated without forming a hydrogel to support the pores. Unlike F100, A100 was practically devoid of visible porosity in the micrograph with a total void area calculated at less than 3%, based on image analysis). Fewer fibrils (white protrusions in the micrographs) related to ductile fracture of the polyethylene matrix appeared in A100, replaced with smoother regions which are believe to correspond to the more brittle dry poly(acrylic acid) phase. It appears that the high applied pressure for this reaction condition provides more efficient movement of the monomer into the matrix compared to F100.

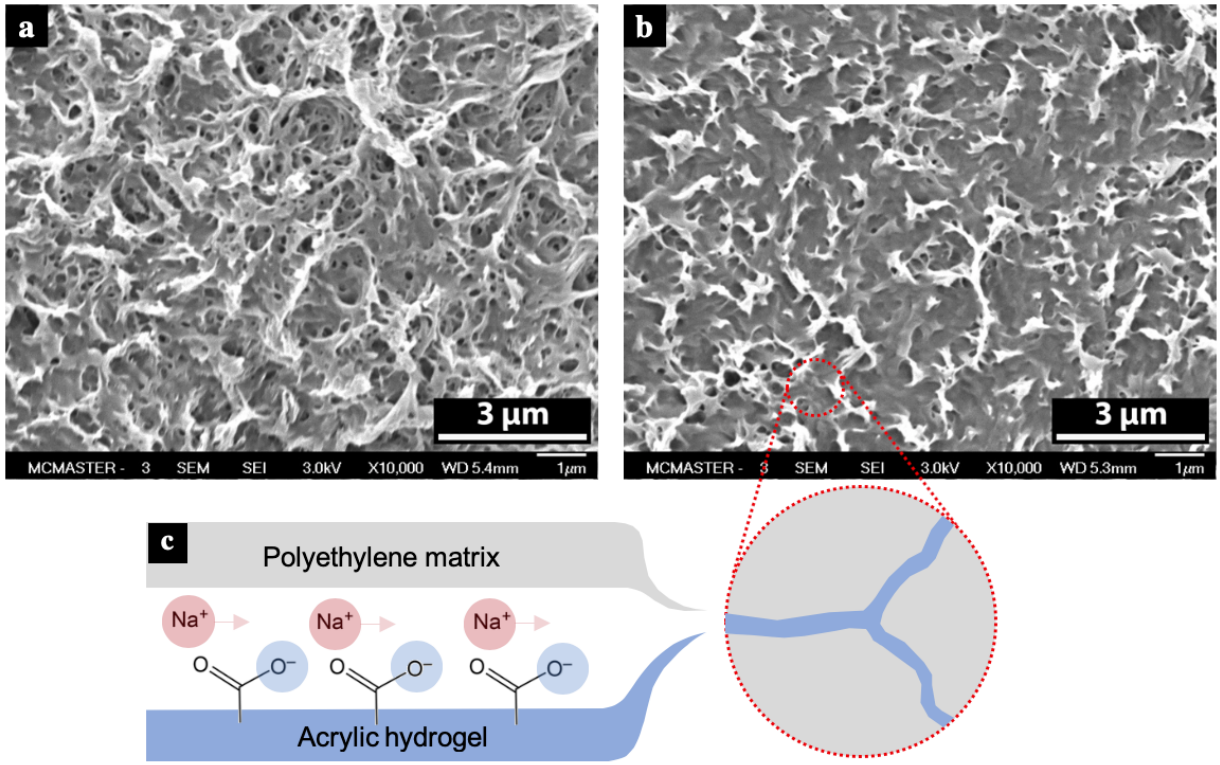

Figure 3. Morphology of the samples that were cryogenically fractured normal to the deformation axis: (a) F100, (b) A100, and (c) schematic representation of the ion transport through the matrix.

Cryo-fracturing was made perpendicular to the sample axis deformation and, therefore, normal to drawing of the craze fibrils. Microimages in Fig. 3 show randomly selected sections of the fracture surface, at a distance of approximately 10 µm from the edge (actual surface of the deformed sample). The images demonstrate consistency in the cavitation pitch, suggesting a similar pattern of matrix deformation. The clearly distinguishable porosity of the sample F100, however, points out the difference in the total content of materials per unit area, which is well-

corresponded with the mass change data. Assuming that the matrix mass is constant, it can be argued that porosity is a discontinuity of the secondary hydrogel phase.

According to microimages, the cavitation of both samples is quite uniform, which is consistent with that obtained by Rozanski et al.,[14] who suppressed gross failure in polymers by exposing them to penetrating liquids while undergoing deformation. The authors showed the positive effect of the liquids' compatibility with the deforming polymers by using hexane and water as the media for polyolefin and polyamide samples, respectively. These observations were taken into account in the present research; the surface energy of matrix polyethylene (0.0353 $N \cdot m^{-1}$ [25]) was quite close to that of the acrylic monomer (0.03 $N \cdot m^{-1}$ [26]).

The effect of liquid on the morphology is explicable from the mechanism of craze formation investigated by Bucknall,[23] according to which the polymer deformation may be accompanied by two processes: initiation of new crazes, and widening (and subsequent fibrillation) of existing ones. The author points out that through the mechanism of fibrillation, a newly formed craze can increase in thickness by a factor of more than 100 while maintaining mechanical stability and not turning into a crack due to the scission of fibrils. Bucknall also explains that the energy required for craze initiation varies with the size of a void, and can be evaluated through the Griffith approach, as a result of which some voids may remain inactive due to their small size. In this case, the sample elongates due to the drawing of fibrils of the existing crazes, which leads to the depletion of chains of the amorphous phase and, ultimately, the samples' failure. In the presence of contact with a liquid, the surface energy of primary voids is decreased, which facilitates their opening. It is useful to note that the contact of polymer with any liquid promotes the new surface formation, which can be observed via Environmental Stress Cracking. However, the greater the compatibility of the penetrating liquid with the matrix polymer, the less energy

that is required for craze initiation. With a sufficient decrease in the energy threshold for the opening of the primary voids, fibrillation can be suppressed with a simultaneous increase in the frequency of the newly formed crazes, due to which the elongation of the sample predominantly occurs. The inner diameter of the resulting channels remains small, which in turn contributes to higher capillary pressure and, therefore, maintains effective penetration of the liquid to the matrix.

Fig. 3a shows a collective effect of the expansion of the crystal-amorphous interface followed by a rise in the number of primary voids, while ensuring contact of the matrix polyethylene with the acrylic monomer. The hierarchical porous structure indicates that primary crazes worked as pathways for monomer delivery, which consequently resulted in the initiation of multiple secondary crazes. However, while wetting the inner surface of the polymer, the monomer did not appear to entirely fill the formed crazes, which is also seen in Fig. 3a. The elevating system pressure was necessary to increase the amount of monomer, allowing more efficient use of the emerged space for the formation of the secondary phase, which is shown by the nearly non-porous cross-section in Fig. 3b.

3.2. MASS CHANGE

Fig. 4 presents the sample mass change for six different pressures, including the case in which the pressure was not applied. In each case, elongations of 50, 75, and 100% are reported. Samples elongated by 25% never showed a statistically significant mass increase for any pressure, showing that the medium did not penetrate the polyethylene matrix without adequate cavitation at the surface. Due to the same lack of change in mass, no data was presented for samples of NI (no initiator) in the figure. The samples of trial F (no pressure) demonstrated the least change related to liquid penetration at any state of strain, with a 1.12% increase in mass by 100%

elongation. With increasing system pressure, there was a corresponding increase in the mass change at each extent of elongation. Such behavior was attributed to induced liquid capillary flow through the restrictive void space with increasing pressure. An inflection was seen within the range of studied elongation for samples of trials C and D, and to a lesser extent for the samples of trials E. This may either suggest that the matrix material becomes more compliant above 75% elongation such that the walls of the existing crazes are being widened more easily, or that more newly initiated crazes are evolved within the cavitated volume thus creating an additional space for the secondary phase propagation. For the trials A and B, however, such an inflection point might be reached earlier (if at all), and so might not be seen within the plot area. The trend with elongation for samples of trials F was also quite linear like trials A and B, reflecting the limited penetration of the solution due to capillary forces and the dynamic viscosity of the liquid for a nominal pore size.

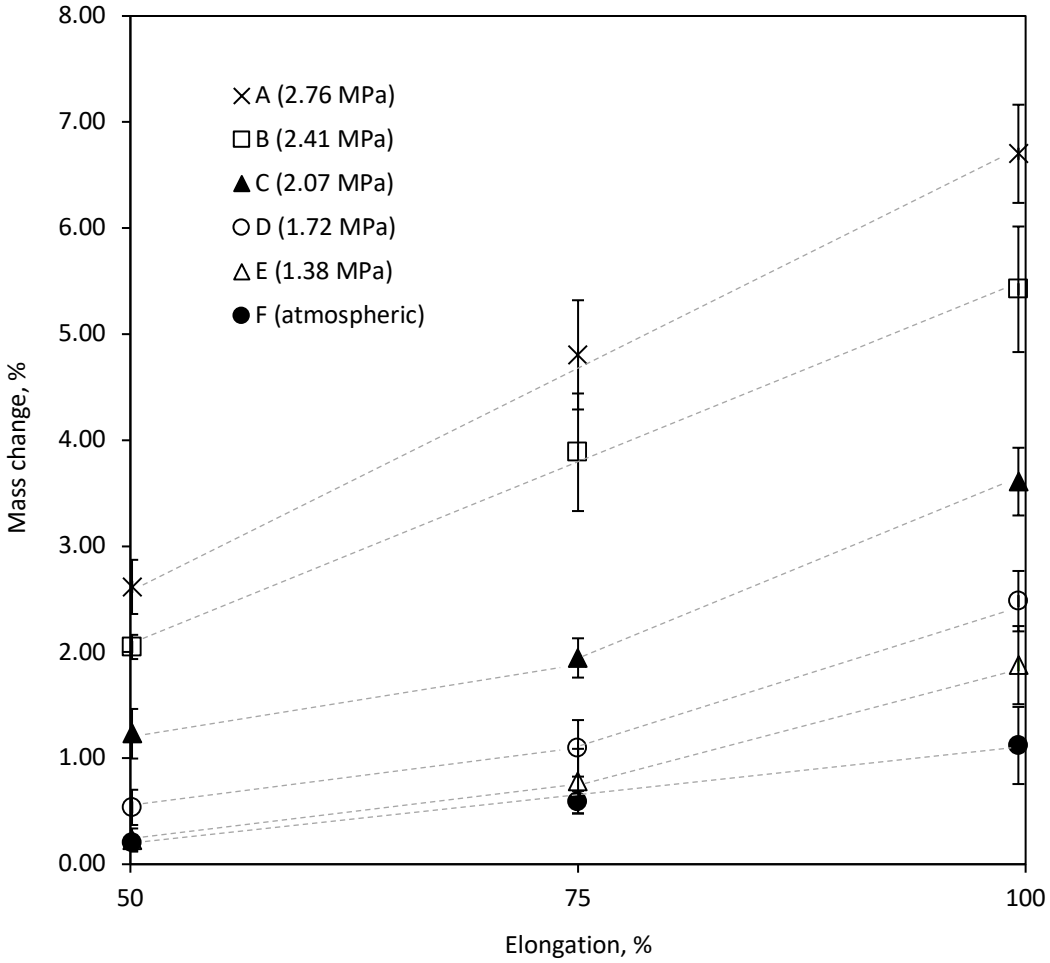

Figure 4. The effect of elongation on the mass change for the different system pressures (gauge). The lines are included to visually highlight transitions perceived in the data.

As a first approximation, these results of an overall mass increase, 1.12% for F100 versus 6.7% for A100, gave an estimate for the total volume of the acrylate phase. They also presented preferable operating conditions in the preparation of the structured alloy; however, like the morphological results already presented, this data did not yet establish whether a percolating network was developed.

3.3. FTIR ANALYSIS

Absorbed water was used as an indicator of the hydrogel in the polyethylene matrix for the infrared analysis in Fig. 5, with a corresponding peak at 3000-3700 cm^{-1}. The broad absorbance peak for water was most intense for the pure hydrogel but still readily observed in the prepared samples. The band corresponding to carboxyl groups at 1652 cm^{-1} was another indicator of the interpenetrating hydrogel, in this case showing that some portion of the functional groups were not neutralized. Comparatively, the visible band for COO^- at 1557 cm^{-1} represented the portion of neutralized hydrogel in the samples.

Samples of trials A and F were microtomed perpendicular to their surfaces to a depth of 10 μm and 50 μm, and analyzed by FTIR. All of the relevant vibrational bands showed weaker absorbances in F100 compared to A100, indicating that a greater concentration of the acrylate secondary phase penetrated the pores when a higher system pressure was used for the reaction. For both trials, a decrease in the band intensity was observed at greater depth from the surface; the reduction of the hydrogel fraction was partially compensated by higher pressure. Thus, for samples of A100 at a depth of 50 μm, the band for COO^- was still clearly distinguishable (Fig. 5c), while for samples F100 at the same depth, the group was not detected (Fig. 5e).

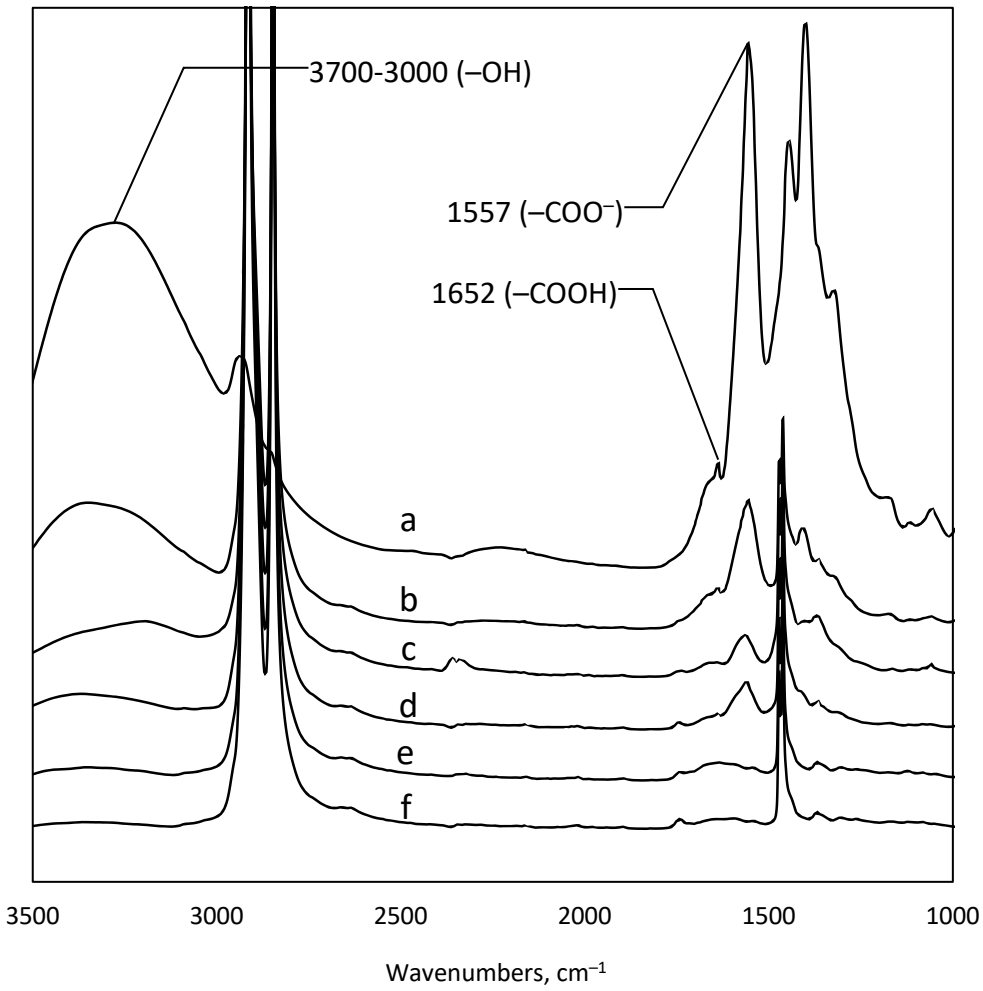

Figure 5. ATR-FTIR spectra: (a) for the reference hydrogel sample, (b) for the sample A100 at a depth of 10 μm, (c) for the sample A100 at a depth of 50 μm, (d) for the sample F100 at a depth of 10 μm, (e) for the sample F100 at a depth of 50 μm, and (f) for the reference matrix polymer sample.

3.4. ELASTIC MODULUS CHANGE

To exhibit conductivity, the acrylate phase must be impregnated with electrolyte, or in other words, the introduced secondary phase has to be swollen with water. In this state, the hydrogel

is rather weak, and does not significantly affect the mechanical properties of the matrix. To avoid variability in the measurements due to evaporation, the dry hydrogel interstitially bound within the polyethylene was tested instead, which being quite rigid might add some additional stiffness to the matrix. Since the two phases lack appreciable bonding to one another, the dispersed phase must have a certain degree of continuity in order to have a noticeable impact on the matrix mechanics. A dry acrylic hydrogel is not conductive; therefore, this data is not operational, and is intended as additional information of evaluation of the morphology of the samples.

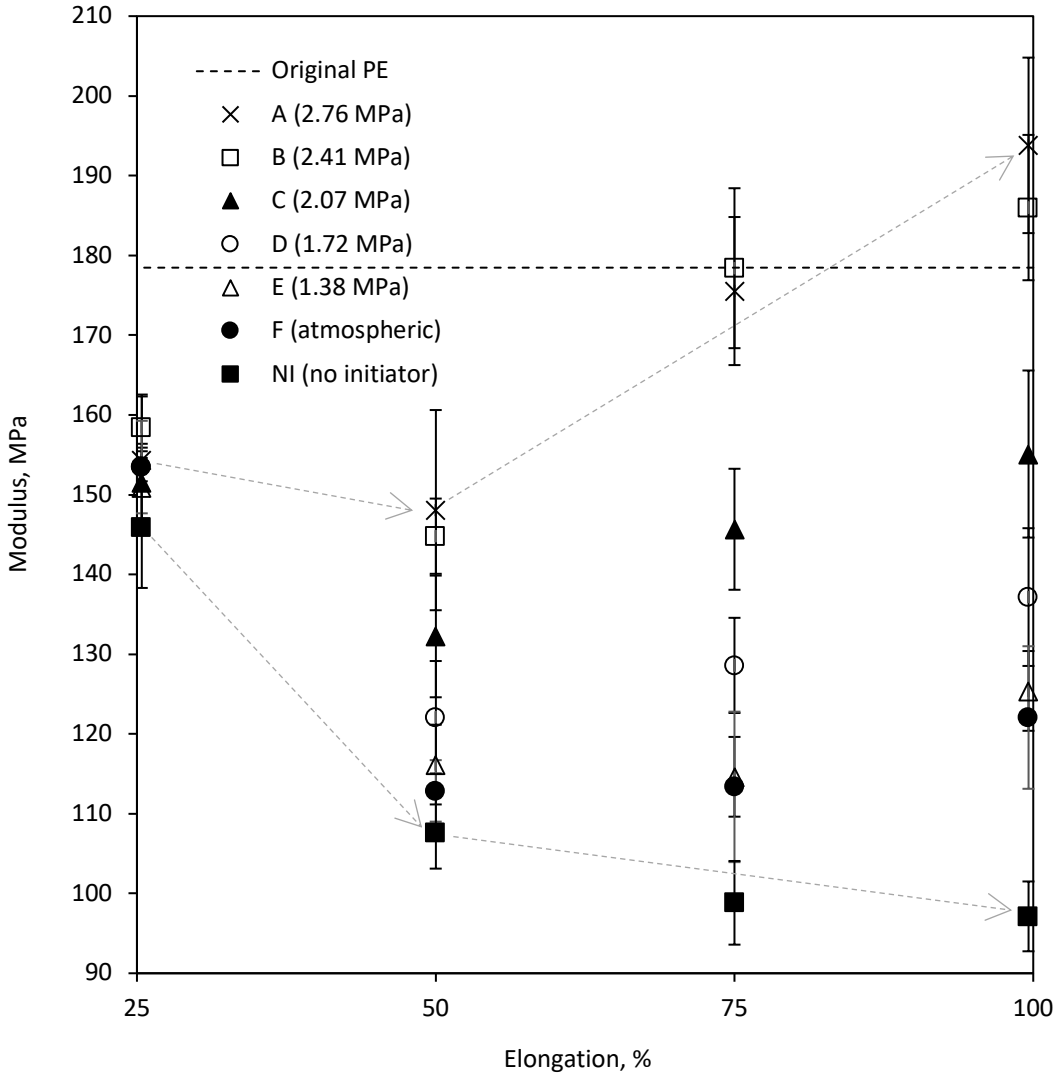

Figure 6. Effect of the elongation and system pressure on Young's modulus of the material. The arrows highlight two extremal results: the upper trend shows the maximum impact of the dispersed phase on stiffness; the lower trend show the absence of an impact by the dispersed phase for the non-polymerized samples for batch NI.

The mechanical results are presented in Fig. 6. An elongation of 25% was accompanied by a decrease in the elastic modulus relative to the original polyethylene, while the system pressure

used at this strain had no significant effect. This suggests weak mutual percolation of initiated crazes, and as a result, a low degree of monomer penetration into the matrix. With further elongation, the modulus decreased by as much as 30% without the secondary phase (based on the results of samples for trial NI), but this loss in stiffness could be compensated with the increasingly interpenetrating polyacrylate structure. This is especially noticeable for the samples of trials A and B, at 75% and 100% elongation, which demonstrated moduli similar or as much as 26% higher than the original polyethylene matrix. Dry PAA itself has a quite high Young's modulus ensured by strong intermolecular interaction and varies from 4.5 to 4.67 GPa. For the neutralized form of PAA, this number has reached as high as 10 GPa.[27]

Slowing down the decrease in the modulus for trial NI could indicate a partial hardening of the matrix due to fibrillation. However, given the presence of a secondary phase for trial A (deformed under the same conditions), it may suggest that fibrillation for trial NI was to a large extent suppressed, as also indicated by the absence of a visible neck of the samples. In this case, the deformation of the samples occurred predominantly due to the formation of secondary crazes, rather than due to widening of existing ones, as was described in the Morphology section.

The mechanical response of the materials showed evidence of an interpenetrating secondary phase at higher pressures and elongation, but this characterization along with the morphology and mass change assessments were insufficient to show the porous system produced by deformation exhibited percolation.

3.5. ION CONDUCTIVITY

While demonstrating the new functionality of the modified polyethylene, the characterization of throughplane ion conductivity was also meant to prove that a co-continuous network (acrylic

hydrogel) had been developed throughout the material from one surface to another. The measure of conductivity was considered to be revealing the quality of the percolating network. The hydrogel was not highly conductive but suitable for the measurement technique, with an inherent conductivity of $5.68 \cdot 10^{-4}$ $S \cdot cm^{-1}$. The reported value is comparable to other studies in the literature.[28]

The ion conductivity of the acrylic hydrogel network within the polyethylene samples is shown in Fig. 7, varying based on the influence of elongation and system pressure during their preparation. The highest conductivity of $4.43 \cdot 10^{-4}$ $S \cdot cm^{-1}$ (median value of three samples tested) was recorded for samples of A100, which was nearly equal to the conductivity of pure hydrogel. The relative standard deviation (RSD) proportionally increased with conductivity and applied pressure, and was 12% nominally. The high value for A100 corresponded with all other analyses that indicated it had the least unfilled voids of all trial conditions, but now there was evidence that those poly(acrylic acid) filled crazes formed a percolating network across the polyethylene substrate, through which the electrolyte could diffuse. The result also allows for the conclusion that the increased modulus of elasticity seen for A100 was indicative of the high level of acrylic phase continuity in polyethylene. Conductivity for the samples of B100 was nearly equal to that for the samples of A100, being $3.93 \cdot 10^{-4}$ $S \cdot cm^{-1}$. In fact, the difference between A100 and B100 was within statistical error. The same trend was observed when comparing the modulus for these two samples, though A100 showed a higher mass change. Thus, a further increase in mass with a certain elongation of the sample does not significantly affect the percolation of the phase; therefore, the additional elevation of pressure was not deemed effective.

It should be noted that conductivity was measured for the undeformed samples, as well as for the samples elongated to 25%, at highest pressure (i.e. A0 – not listed in the table, and A25).

However, the results showed no conductivity for these two conditions and were thus not included in the graph. Since there was no network formed in the matrix, no throughplane conductivity was measured. The samples of trial NI also remained nonconductive at the elongation to 50% and less. Some conductivity was detected only at 75% and 100% elongation, though at the lower detection threshold of the multimeter, which might suggest either trace amounts of monomer, or slight diffusion of electrolyte through cavitated matrices.

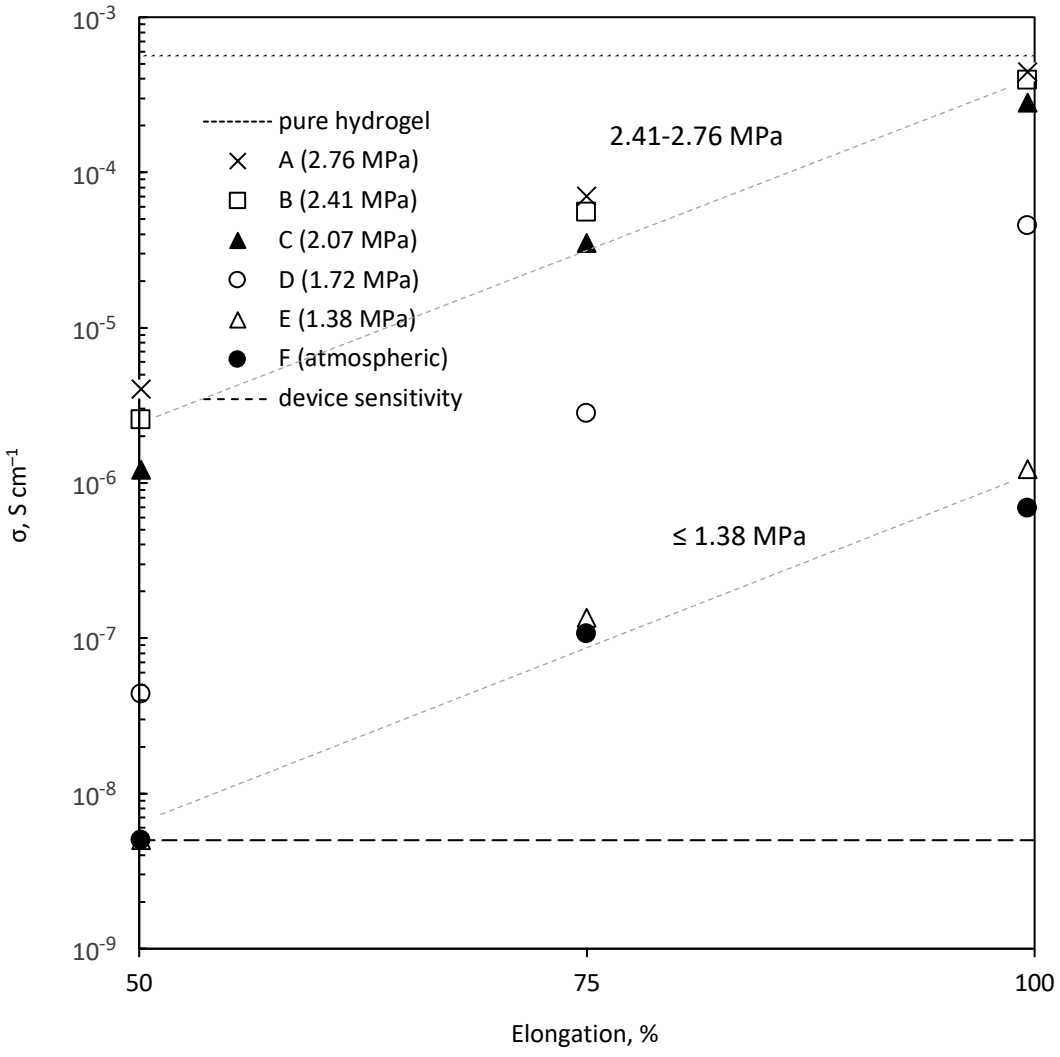

Figure 7. Conductivity of the samples deformed at different pressures as a function of elongation. Gray lines show two distinctive extremal trends in conductivity, and the transition region

between them. RSD proportionally increased with conductivity and applied pressure, and was of 12% in average.

The transition in the experimental conditions between trials A/B/C versus D, produced a decline in conductivity. Based on the results, trial C was considered to represent the lowest structural variation to produce an interpenetrating network, though its modulus and mass change was notably lower; a plateau in performance is expected for properties reliant on a percolation network once sufficient continuity in the hydrogel across the polyethylene was reached.

4. CONCLUSION

The mechanism of crazing in polymers under tensile deformation was used to form continuous submicron-size channels in the matrix of a commodity polymer, enabling the material to exhibit through-plan conductivity by a newly polymerized hydrogel phase. The liquid monomeric medium was found to function as both surface-active agent for craze initiation, as well as the secondary phase for the subsequent polymerization. Elevated pressures were found beneficial to overcome capillary forces and promote deep penetration of the medium into the crazed matrix, to ensure continuity in properties while minimize the extent of mechanical losses in the new material. Collectively, these results demonstrate the potential of modifying regular semicrystalline polymers, such as commodity polyethylene, so as to impart them conductivity.

ACKNOWLEDGEMENT

The authors sincerely acknowledge the Natural Science and Engineering Research Council (NSERC) of Canada for supporting this fundamental research through Discovery Grant program.

We also thank the Canada Foundation for Innovation (CFI) for the equipment and facilities. S.Z. thanks the Canada Research Chair (CRC) program for supporting his research.

REFERENCES

(1) Jonsson, A.; Song, Z.; Nilsson, D.; Meyerson, B. A.; Simon, D. T.; Linderoth, B.; Berggren, M. Therapy Using Implanted Organic Bioelectronics. *Sci. Adv.* **2015**, *1* (4), e1500039. https://doi.org/10.1126/sciadv.1500039.

(2) Simon, D. T.; Kurup, S.; Larsson, K. C.; Hori, R.; Tybrandt, K.; Goiny, M.; Jager, E. W. H.; Berggren, M.; Canlon, B.; Richter-Dahlfors, A. Organic Electronics for Precise Delivery of Neurotransmitters to Modulate Mammalian Sensory Function. *Nat. Mater.* **2009**, *8* (9), 742–746. https://doi.org/10.1038/nmat2494.

(3) Jonsson, A.; Sjöström, T. A.; Tybrandt, K.; Berggren, M.; Simon, D. T. Chemical Delivery Array with Millisecond Neurotransmitter Release. *Sci. Adv.* **2016**, *2* (11), e1601340. https://doi.org/10.1126/sciadv.1601340.

(4) Hoare, T. R.; Kohane, D. S. Hydrogels in Drug Delivery: Progress and Challenges. *Polymer (Guildf).* **2008**, *49* (8), 1993–2007. https://doi.org/10.1016/J.POLYMER.2008.01.027.

(5) Shin, S. R.; Bae, H.; Cha, J. M.; Mun, J. Y.; Chen, Y.-C.; Tekin, H.; Shin, H.; Farshchi, S.; Dokmeci, M. R.; Tang, S.; et al. Carbon Nanotube Reinforced Hybrid Microgels as Scaffold Materials for Cell Encapsulation. *ACS Nano* **2012**, *6* (1), 362–372. https://doi.org/10.1021/nn203711s.

(6) Saez-Martinez, V.; Garcia-Gallastegui, A.; Vera, C.; Olalde, B.; Madarieta, I.; Obieta, I.; Garagorri, N. New Hybrid System: Poly(Ethylene Glycol) Hydrogel with Covalently Bonded Pegylated Nanotubes. *J. Appl. Polym. Sci.* **2011**, *120* (1), 124–132. https://doi.org/10.1002/app.33095.

(7) Maranchi, J. P.; Trexler, M. M.; Guo, Q.; Elisseeff, J. H. Fibre-Reinforced Hydrogels with High Optical Transparency. *Int. Mater. Rev.* **2014**, *59* (5), 264–296. https://doi.org/10.1179/1743280414Y.0000000032.

(8) Eslami, M.; Vrana, N. E.; Zorlutuna, P.; Sant, S.; Jung, S.; Masoumi, N.; Khavari-Nejad, R. A.; Javadi, G.; Khademhosseini, A. Fiber-Reinforced Hydrogel Scaffolds for Heart Valve Tissue Engineering. *J. Biomater. Appl.* **2014**, *29* (3), 399–410. https://doi.org/10.1177/0885328214530589.

(9) Visser, J.; Melchels, F. P. W.; Jeon, J. E.; van Bussel, E. M.; Kimpton, L. S.; Byrne, H. M.; Dhert, W. J. A.; Dalton, P. D.; Hutmacher, D. W.; Malda, J. Reinforcement of Hydrogels Using Three-Dimensionally Printed Microfibres. *Nat. Commun.* **2015**, *6* (1), 6933. https://doi.org/10.1038/ncomms7933.

(10) Pati, F.; Jang, J.; Ha, D.-H.; Won Kim, S.; Rhie, J.-W.; Shim, J.-H.; Kim, D.-H.; Cho, D.-W. Printing Three-Dimensional Tissue Analogues with Decellularized Extracellular Matrix Bioink. *Nat. Commun.* **2014**, *5* (1), 3935. https://doi.org/10.1038/ncomms4935.

(11) Bernier, G. A.; Kambour, R. P. The Role of Organic Agents in the Stress Crazing and Cracking of Poly(2,6-Dimethyl-1,4-Phenylene Oixde). *Macromolecules* **1968**, *1* (5), 393–400. https://doi.org/10.1021/ma60005a005.

(12) Volynskii, A. L.; Aleskerov, A. G.; Grokhovskaya, T. Y.; Bakeyev, N. F. Mechanical Behavior of Glassy Polyethylene Terephthalate Deformed in Liquid Adsorption Active Media. *Polym. Sci. USSR* **1976**, *18* (9), 2419–2426.

(13) Volynskii, A. L.; Bakeev, N. F. *Solvent Crazing of Polymers*; Newnes, 2012; Vol. 13.

(14) Rozanski, A.; Galeski, A. Plastic Yielding of Semicrystalline Polymers Affected by Amorphous Phase. *Int. J. Plast.* **2013**, *41*, 14–29. https://doi.org/10.1016/J.IJPLAS.2012.07.008.

(15) Rozanski, A.; Galeski, A. Controlling Cavitation of Semicrystalline Polymers during Tensile Drawing. *Macromolecules* **2011**, *44* (18), 7273–7287.

(16) Weichold, O.; Goel, P.; Lehmann, K.-H.; Möller, M. Solvent-Crazed PET Fibers Imparting Antibacterial Activity by Release of Zn^{2+}. *J. Appl. Polym. Sci.* **2009**, *112* (5), 2634–2640. https://doi.org/10.1002/app.29818.

(17) Trofimchuk, E. S.; Nikonorova, N. I.; Chagarovskii, A. O.; Volynskii, A. L.; Bakeev, N. F. Crystallization of Silver Chloride in Crazed Porous Polymers. **2005**. https://doi.org/10.1021/JP051920C.

(18) Rukhlya, E. G.; Litmanovich, E. A.; Dolinnyi, A. I.; Yarysheva, L. M.; Volynskii, A. L.; Bakeev, N. F. Penetration of Poly(Ethylene Oxide) into the Nanoporous Structure of the Solvent-Crazed Poly(Ethylene Terephthalate) Films. *Macromolecules* **2011**, *44* (13), 5262–5267. https://doi.org/10.1021/ma200812c.

(19) Rukhlya, E. G.; Karpushkin, E. A.; Yarysheva, L. M.; Volynskii, A. L. Special Features of Crazing of Glassy Poly(Ethylene Terephthalate) in Poly(Ethylene Oxide) Solutions.

Macromolecules **2017**, *50* (14), 5459–5465. https://doi.org/10.1021/acs.macromol.7b01084.

(20) Yarysheva, A. Y.; Bagrov, D. V.; Bakirov, V. A. V.; Tarasevich, B. N.; Grohovskaya, T. E.; Yarysheva, L. M.; Chvalun, S. N.; Volynskii, A. L. Polyethylene–Poly(Ethylene Oxide) Hybrid Films Obtained by Crazing and Their Structural Peculiarities. *Macromolecules* **2017**, *50* (7), 2881–2888. https://doi.org/10.1021/acs.macromol.6b02512.

(21) Pawlak, A.; Galeski, A. Stability of Spherulite Growth Rate. *J. Polym. Sci. Part B Polym. Phys.* **1990**, *28* (10), 1813–1821. https://doi.org/10.1002/polb.1990.090281012.

(22) Nowacki, R.; Kolasinska, J.; Piorkowska, E. Cavitation during Isothermal Crystallization of Isotactic Polypropylene. *J. Appl. Polym. Sci.* **2001**, *79* (13), 2439–2448. https://doi.org/10.1002/1097-4628(20010328)79:13<2439::AID-APP1051>3.0.CO;2-#.

(23) Bucknall, C. B. New Criterion for Craze Initiation. *Polymer (Guildf).* **2007**, *48* (4), 1030–1041. https://doi.org/https://doi.org/10.1016/j.polymer.2006.12.033.

(24) Pawlak, A.; Galeski, A.; Rozanski, A. Cavitation during Deformation of Semicrystalline Polymers. *Prog. Polym. Sci.* **2014**, *39* (5), 921–958. https://doi.org/10.1016/J.PROGPOLYMSCI.2013.10.007.

(25) Federal Republic of Germany. Surface Tension Values of Some Common Polymers/Test Liquids for Surface Energy Analysis www.surface-tension.de.

(26) Gokel, G. W.; Dean, J. A. *Dean's Handbook of Organic Chemistry*; McGraw-Hill handbooks; McGraw-Hill, 2004.

(27) Cappella, B. *Mechanical Properties of Polymers Measured through AFM Force-Distance Curves*; Springer Laboratory; Springer International Publishing: Cham, 2016. https://doi.org/10.1007/978-3-319-29459-9.

(28) Pochard, I.; Couchot, P.; Foissy, A. Potentiometric and Conductometric Analysis of the Binding of Barium Ions with Alkali Polyacrylate. *Colloid Polym. Sci.* **1998**, *276* (12), 1088–1097. https://doi.org/10.1007/s003960050350.

Graphical abstract